Journal of Applied Physics

AIP Publishing

Interface and layer periodicity effects on the thermal conductivity of copper-based nanomultilayers with tungsten, tantalum, and tantalum nitride diffusion barriers

Claudia Cancellieri,[1, a)] Ethan A. Scott,[2, a)] Jeffrey Braun,[2] Sean King,[3] Ron Oviedo,[3] Christopher Jezewski,[3] John Richards,[3] Fabio La Mattina,[1] Lars P.H. Jeurgens,[1] and Patrick E. Hopkins[2, 4, 5, b)]

[1)]*Empa, Swiss Federal Laboratories for Materials Science and Technology, Überlandstrasse 129, 8600 Dübendorf, Switzerland.*

[2)]*Department of Mechanical and Aerospace Engineering, University of Virginia, Charlottesville, VA 22904*

[3)]*Logic Technology Development, Intel Corporation, Hillsboro, Oregon 97124, USA*

[4)]*Department of Materials Science and Engineering, University of Virginia, Charlottesville, VA 22904*

[5)]*Physics Department, University of Virginia, Charlottesville, VA 22904*

Nanomultilayers are complex architectures of materials stacked in sequence with layer thicknesses in the nanometer range. Their application in microelectronics is challenged by their thermal stability, conductivity and interface reactivity which can compromise their performance and usability. By using different materials as thermal barriers and by changing their thickness, it is possible to manipulate interfacial effects on thermal transport. In this work, we report on the thermal conductivity of Cu/W, Cu/Ta, and Cu/TaN sputter deposited nanomultilayers with different thicknesses. The resistive interfacial effects are rationalized and discussed also in relation to the structural transformation into a nano-composite upon high temperature annealing.

I. INTRODUCTION

Nanomultilayers (NMLs) represent an important class of nanomaterials, which find numerous applications in the fields of micro and nano electronic, optical, medical and sensing devices. These nano-architectures can be made functional, and their mechanical, chemical and/or physical properties can be tailored through microstructural and interfacial design. Currently, Cu/W, Cu/Ta, and Cu/TaN remain among the most ubiquitous multilayers used in interconnect systems, which can be attributed to longstanding fabrication infrastructures, cost considerations, and scalability[1–10]. Despite the capability of manufacturing smaller period thicknesses, reduced device dimensions give rise to several engineering challenges. For example, NML systems are known to be intrinsically thermodynamically unstable as compared to their respective bulk materials, due to the high amount of excess energy contributions arising from internal interfaces (i.e. phase and grain boundaries) and internal residual stresses[11–13]. Furthermore, the interfaces in these systems strongly affect the thermal properties and yield a reduced thermal conductivity in comparison to the pure constituent bulk materials.

With regard to the influence of interfaces on structural and thermal stability, a number of recent studies have highlighted the advantages and challenges associated with copper-based NMLs. For example, Xue *et al.*[14] investigate the role of period thickness on the thermal stability of Cu/W NMLs, demonstrating a reduction in mechanical integrity amongst the thinnest periods. Correspondingly, Dong *et al.*[15], have reported a significant reduction in the thermal conductivity of Cu/W multilayers scaling with period thickness, which is largely attributed to a reduction of interface coherence. In other copper-based multilayers, including Cu/Ta, Powers *et al.*[16], have demonstrated that hillock formation at elevated temperatures can exacerbate the issue of loss of interface coherence.

For layer thicknesses on the order of carrier mean free paths, interface resistance becomes a critical impediment to heat transfer[17,18]. In the case of NMLs consisting of constituent layers of different material or phase, this can arise from the combination of poor mechanical or chemical adherence at the interface and a thermal expansion mismatch between the constituent layers, inhibiting the transfer of vibrational energy across the interface. While lowering effective thermal conductivity by adding interfaces is advantageous for thermoelectric and thermal barrier coating applications, it is undesirable for microelectronic applications where there is a need to dissipate ever increasing amounts of waste heat. Moreover, the thermal resistance of interfaces degrades the performance of materials intended for thermal management, such as polycrystalline diamond[19] and nanoscale composites[20]. It is then clear that a trade-off should be sought among different combinations of metallic and barrier materials depending on the final application.

In this work, we report a systematic comparison between the thermal conductivity of Cu-based nanomultilayers with different barrier layers: Ta, TaN, and W. The thermal boundary conductance (TBC) is derived through a series resistance model and is discussed in relation to the interface density and layer thickness. For further insight into microstructural effects on thermal transport within the NMLs, samples are additionally annealed until the point of layer diffusion. At sufficiently high temperatures, the NMLs composed of alternating metallic and barrier layers are found to degrade into nanocomposites (NCs). Starting from a NML structure of alternating, immiscible metals, the high-temperature thermal degradation of

[a)]Claudia Cancellieri and Ethan A. Scott contributed equally to this work

[b)]Electronic mail: phopkins@virginia.edu

the NML proceeds by thermal grooving of grain boundaries, pinching-off of the nanolayers and subsequent spheroidization of residual layer-fragments, leading to a NC formation[21–24]. The NML to NC transformation is accompanied by complete stress relaxation in both layers[22,23].

The results of this study provide useful insight for a number of engineering disciplines as understanding of thermal transport in nano- sized features is critical for next generation device functionality including multilayered structures. Furthermore, while the majority of works investigating the effects of interfacial resistances on thermal transport have focused upon non-metal/non-metal or metal/non-metal interfaces, considerably fewer works have been focused upon metal/metal interfaces in which thermal transport is electron dominated, and Kaptiza conductances are much higher[25–28].

II. EXPERIMENTAL PROCEDURE

A. Material deposition

The Cu/Ta and Cu/TaN multilayers were deposited on 300 mm diameter Si (001) substrates using an industry standard physical vapor deposition (PVD) tool[29]. Prior to Cu/Ta(N) multilayer formation, a 100 nm thick thermal oxide was grown on the Si (001) substrate followed by plasma enhanced chemical vapor deposition (PECVD) of 100 nm thick SiN and 25 nm thick PVD Ta(N) adhesion layers. An approximately 400 nm Cu buffer layer was subsequently deposited by combined PVD and electroplating methods followed by a chemical mechanical polish to planarize and reduce the Cu layer to a final layer thickness of 300 nm. The Cu/Ta(N) multilayers were subsequently deposited on the 300 nm Cu by PVD with period thicknesses ranging from 5 – 40 nm. The Cu/Ta(N) layers were fabricated on the 300 nm thick Cu layer to mimic the use of Ta and TaN as diffusion barriers in microelectronic Cu metal interconnects.Cu/W NMLs were deposited on 2″ α-Al_2O_3 and Si single-crystalline substrates, sapphire-C (0001) and Si (100)+ 15 nm of Si_3N_4 wafers, by DC unbalanced magnetron sputtering in a high vacuum chamber (base pressure $< 10^{-8}$ mbar) from two 2″ targets of pure W (99.95%) and Cu (99.99%) confocally arranged and operated at 200 Watts. Before insertion in the deposition apparatus, the sapphire substrates were ultrasonically cleaned using acetone and ethanol. Prior to deposition, possible surface contamination on the α-Al_2O_3 substrates (mostly adventitious carbon) was removed by Ar^+ sputter cleaning for 5 min applying a RF bias of 100 V. First, a 25 nm-thick W buffer layer was deposited on the sputter-cleaned substrate. Next, 100 repetitions of alternating Cu and W layers with a different (nominal) thickness of 5, 3 and 10 nm were deposited on top. For the heat treatment, select as-prepared samples were isothermically annealed *ex-situ* at temperatures ranging from 500 to 800 °C for 100 min in vacuum ($< 10^{-5}$ mbar)[21,23]. For clarity of sample structure, a schematic of each NML system is shown in Fig. 1. For further details on individual samples, we refer the reader to Table S3 of the supplementary material.

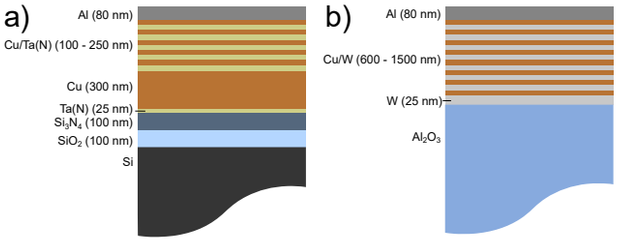

FIG. 1. Representative schematic of the layer contents, with nominal thickness, are displayed in a) and b) for the Cu/Ta(N) and Cu/W NML systems, respectively.

B. Characterization

A Bruker D8 Discover X-ray diffractometer, operated in Bragg-Brentano geometry, was used to measure 2-theta (2θ) scans for the as-deposited and annealed samples. To access the texture, pole figures of Cu $\{111\}$ and Ta/TaN $\{110\}$ family of planes were recorded in point focus geometry. XRD scans and texture measurements were measured at room temperature on *ex-situ* annealed samples.

For thermal property characterization, the samples were coated with an 80 nm film of Al to serve as a transducer for time domain thermoreflectance (TDTR). In short, TDTR is a non-contact optical pump probe technique which is used to monitor the change in reflectance of a sample surface in response to a modulated heating event. The output of an ultrafast pulsed laser is split into a pump and probe path: the pump path is modulated at a particular frequency, ultimately inducing the modulated heating event at the coated sample surface. The probe path is concentrically focused onto the sample surface with the pump, and the impingement upon the sample surface of the pulsed probe can be delayed relative to that of the pump via a mechanical delay stage, enabling high temporal resolution. For our measurements, we utilize a Ti:sapphire laser with a repetition rate of 80 MHz with a central wavelength of 800 nm and bandwidth of 11 nm. The pump path is frequency doubled to 400 nm with a bismuth triborate (BIBO) crystal, and modulated at 10 MHz using an electro-optic modulator.

The modulated response of the reflected probe is monitored with a lock-in amplifier as a function of delay time. As the measured change in reflectance is directly proportional to the change in temperature of the surface, the reflectivity decay as a function of time can be fit with a thermal model[30–33], with the parameters of interest used as fitting parameters in the model (typically thermal conductivity, κ, or thermal boundary conductance, G). As there are numerous layers within the system, and because we are interested in the overall thermal conductivity of the multilayer region, we treat the multilayer region as a single continuum within the sample stack. The dimensions of the sample stacks are determined through cross sectional scanning electron microscopy (XSEM). For the Cu/Ta and Cu/TaN samples, the sample stack is considered as a seven-layer model comprising of: an 80 nm Al capping layer, a 100 - 250 nm multilayer region, 300 nm copper

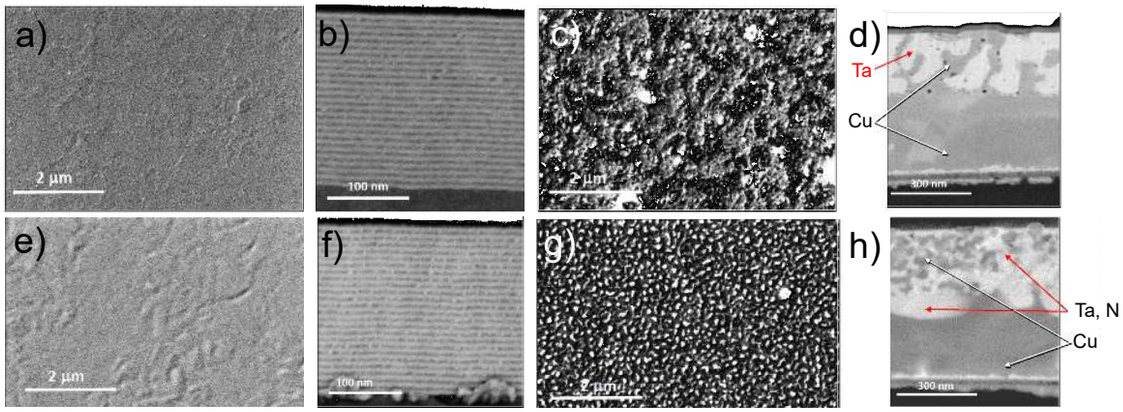

FIG. 2. Plan-view and cross sectional SEM images of the as deposited (a, b, e, and f) and annealed (c, d, g, h) NMLs. Cu/Ta is displayed in a - d, whereas Cu/TaN is displayed in e - h. For these images, the NMLs consist of 5nm/5nm layers repeated 25 times, and correspondingly after annealing at 800 °C.

buffer layer, 25 nm Ta(N) adhesion layer, 100 nm SiN adhesion layer, and a 100 nm SiO_2 oxide layer all atop a silicon substrate. The Cu/W samples, fabricated upon Al_2O_3 substrates, are represented by a four-layer model: an Al capping layer, the multilayer region, and a TaN buffer layer atop the Al_2O_3 substrates. The thickness of the Cu buffer layers, as well as the Ta(N) buffer layers are determined from XSEM measurements. Beneath the Ta(N) there is reduced sensitivity to particular layer thickness (see supplementary material, Figure S2), and the nominal thicknesses of the Si_3N_4 and SiO_2 layers are utilized. The heat capacity of the multilayer region is calculated by applying a rule of mixtures formulation with the heat capacity values of the constituent layers. The heat capacity and thermal conductivity of the other films are assumed from literature; particular parameters for each layer in the thermal model are outlined in Table I.

The thermorelectance data for these NMLs is analyzed in the same method as Cheaito *et al.*[25], who previously analyzed Cu/Nb multilayers, by treating the thermal conductivity of the multilayer region and interface between the Al transducer and multilayer region as fitting parameters in the thermal model, and neglecting the interface resistances for layers underneath the multilayer region. We verify our sensitivity to the thermal resistance of each layer by performing sensitivity analyses in the method of Gundrum *et al.*[26] and find that the measurements are most sensitive to the thermal conductivity of the multilayer region, as it is the most thermally resistive region within the sample. Sensitivity analyses as a function of both delay time and modulation frequency are provided in the supplementary material (Figure S2).

TABLE I. Thickness (d), thermal conductivity (κ) and volumetric heat capacity (C_v) values used in the thermal model of the TDTR data. The thermal conductivity of the multilayer region as well as the thermal boundary conductance were used as fitting parameters within the model. Thermal properties of the other layers within the system are taken from literature and referenced accordingly.

System	Layer	Material	d (nm)	C_v (MJ m^{-3} K^{-1})	κ (W m^{-1} K^{-1})
Cu/Ta(N)					
	1	Al	80	2.43[34–36]	135[36,37]
	2	Cu/Ta(N)	110 - 238	2.89 - 3.13	Fig. 5
	3	Cu	268 - 304	3.45[38]	398[39,40]
	4	TaN	22 - 31	2.18[41]	3[42]
	5	SiN	100	2.1[43,44]	2.1[45]
	6	SiO_2	100	1.65[36,44]	1.35[36]
	7	Si	bulk	1.65[36]	140[46]
Cu/W					
	1	Al	80	2.43[34–36]	135[36,37]
	2	Cu/W	600 - 1500	3.02 - 3.25	Fig. 5
	3	W	25	2.56[47]	52.2[48]
	4	Al_2O_3	bulk	3.02[34]	35[46]

III. RESULTS AND DISCUSSION

A. Microstructure

The microstructure of the as-deposited and annealed NMLs were investigated by SEM analysis; micrographs of the as-deposited and 800 °C heat-treated NML are shown in Fig. 2, (both in plan and cross-sectional view). The surface of the as-deposited NMLs demonstrates uniformity and exhibits a grain-like morphology (as originating from the waviness of the deposited nanolayers; see Ref. 21) with no evidence of cracks, voids and/or delaminations (Fig. 2a and e). The average surface roughness (R_a) derived by AFM (see supplementary materials) is always equal or less than 2 nm, indicating a smooth flat surface. In cross-sectional view, the 300 nm thick Cu bottom layer and the periodicity of the alternating Cu/Ta, TaN layers is clearly resolved (Fig. 2b, f), with the deposited nanolayers maintaining relative uniformity across the entire thickness. After annealing at 800 °C, the surface morphology changes drastically (fig. 2c, g). The R_a is now around 70-80 nm (See supplementary materials), considerably increased with respect to the as deposited state and the original stratified structure degrades into a nanocomposite structure, con-

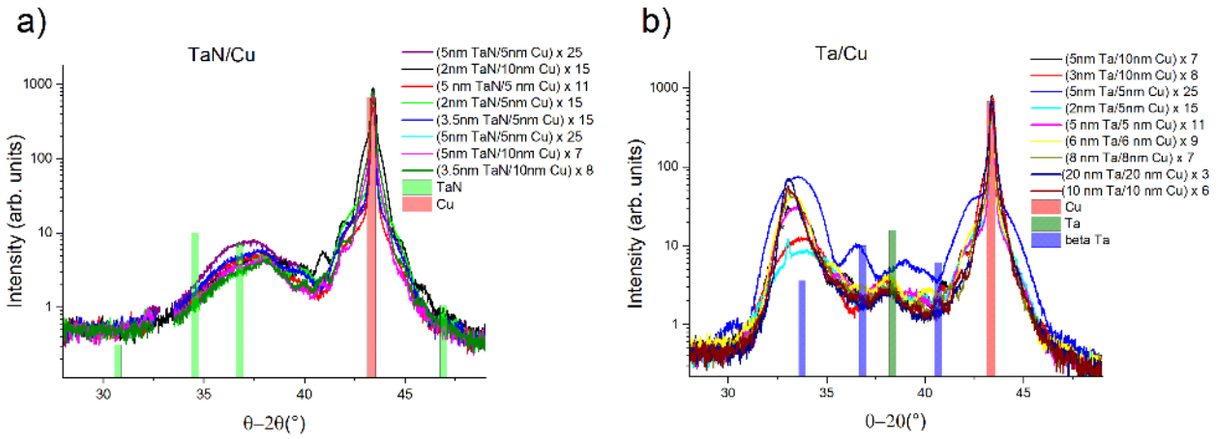

FIG. 3. XRD on the series of a) Cu/Ta and b) Cu/TaN NMLs with different thicknesses. The Cu, Ta and TaN references are also indicated.

sisting of globular Ta,TaN agglomerates embedded in a Cu matrix (Fig. 2d, h). The elemental composition of the different region in 2d, h) has been derived by EDX analysis. SEM analysis of Cu/W NMLs before and after heat treatment has been extensively performed and reported in Refs. 21,23. The NML to nano-composite transformation was found to occur at $T > 750$°C resulting in the formation of NCs, consisting of W particles in a Cu matrix, and the microsctructure of the degraded NML is found to depend strongly on the layer thickness and number of repetitions of the original nanolayers.

XRD analysis of the as-deposited mulitlayers of Cu/Ta is shown in Fig. 3. In the supplementary material, the XRD measurements of the single Ta and Cu layers are also presented (Fig.S1). The Cu buffer layer is polycrystalline with a [111] texture, typical of Cu sputtered PVD films[49]. The Ta layer grown on the Cu buffer layer is primarly composed of the β-Ta phases with [001] preferential growth direction. The more common α-Ta can hardly be distinguished in the as deposited state and becomes evident only after annealing at 600° C (see next paragraph). The Cu/Ta multilayers present the typical intensity modulation of periodic superlattices[50]; the oscillations are compatible with the β-Ta phase oriented along the [001] direction and the Cu layers oriented along [111], superimposed on the narrower Cu(111) peak from the buffer layer. Similarly, the Cu/TaN NMLs, show preferential growth directions of [111] and [101] for the Cu and TaN layers, respectively. The as-deposited multilayers show similar XRD patterns independent of the layer thickness and period. No clear satellite peaks and pronounced finite size oscillations are observed indicating similar disorder and defect concentration in the initial NMLs state. The TaN broad peak in the as deposited scan (Fig. 4d) corresponds to the (101) bragg reflection. The Cu/TaN NMLs appear to be more disordered with broader and less intense peaks in the as-deposited state, compared to Cu/Ta NMLs. The pole figure in Fig.4a confirms the polycrystallinity of Cu with a preferential [111] orientation with a fiber texture (rotational symmetry) in-plane. The β-Ta $\{110\}$ pole figure also presents an in-plane fiber texture and 2 rings: one more pronounced at a tilt angle of $\sim 65°$ and a lower intensity ring at 30°. The most intense ring corresponds to the angle between the $\{110\}$ planes and the [001] direction confirming the preferential orientation of the Ta layers along [001]. The TaN pole figure in Fig.4b confirms the disordered and partially amorphous nature of the TaN layer: only diffuse intensity is observed and no poles neither rings are observed at any tilt angles.

In Figs. 4c and d, the structural evolution of the NMLs with temperature is reported. Up to an annealing temperature of 600 °C, no distinct structural changes are detected by XRD. Pronounced structural transformations are observed for both samples (i.e. Ta and TaN), with and without N, for annealing temperatures $T \geq 700$°C. The β-Ta in Cu/Ta NMLs transforms into α-Ta phase after annealing at 600 °C (Fig. 4c). Moreover, at 800 °C, the formation of Ta silicate phases are observed. On the contrary, no silicate phase formation is observed in Cu/TaN NMLs after high temperature annealing, demonstrating that TaN is a better Si diffusion barrier, which is in accordance with the literature[51,52]. For the Cu/TaN NMLs, the TaN layers are polycrystalline and a substoichiometric cubic phase develops during the annealing. In particular, the $TaN_{0.5}$ phase is formed at 700 °C and additionally, at 800 °C, the $Ta_{0.75}N$ phase is formed in coexistence with the $TaN_{0.5}$ phase. In the Cu/W NMLs, the periodic structure is preserved up to 700 °C and for the individual layer thickness of 10 nm, the multilayer structure is maintained up to 800 °C[21,23]. If the Cu or W layer thickness is less than 10 nm, the NML structure is completely destroyed after annealing at $T \geq 750$ °C and the system is transformed into NCs. In the following section, we compare the thermal conductivity of all the annealed NMLs: after 800 °C annealing, all the systems are completely transformed into NCs.

B. Thermal conductivity and thermal boundary conductance

The results of the TDTR measurements for the thermal conductivity of the multilayer regions are plotted in Figure 5 as a

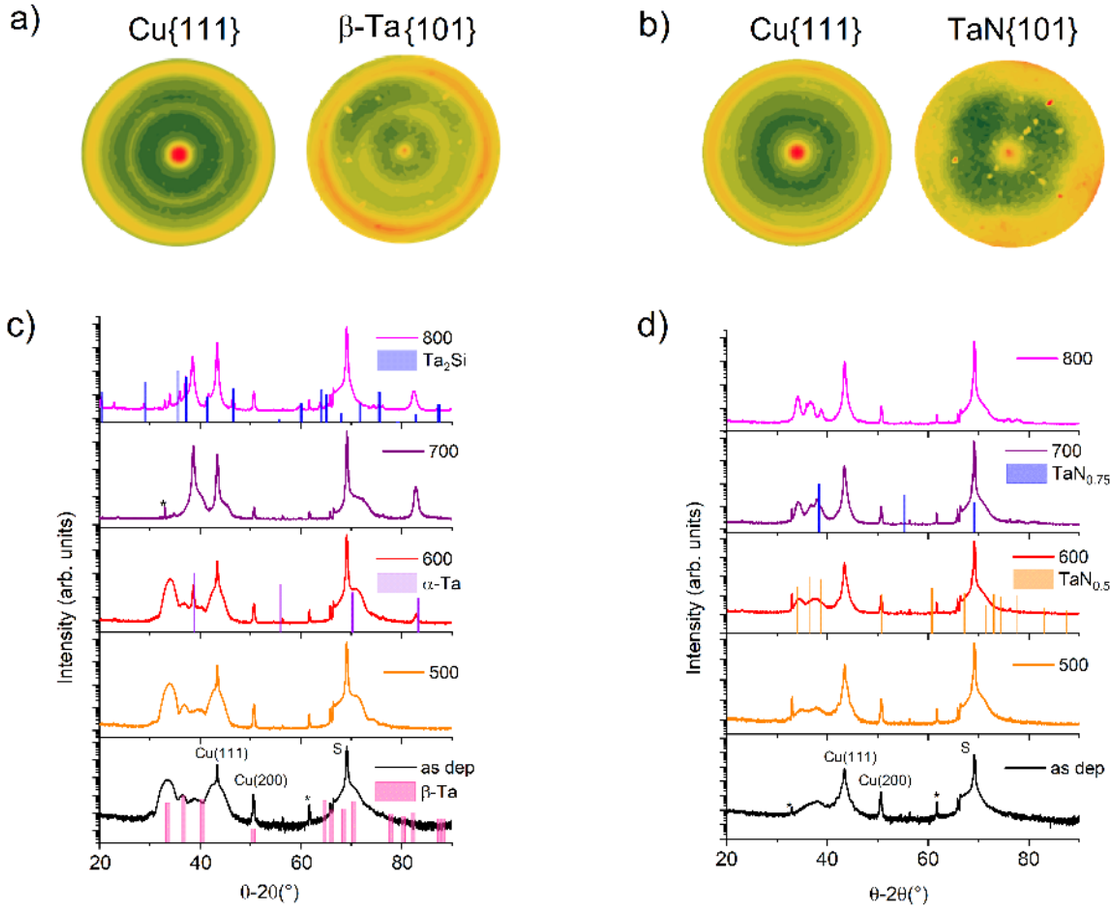

FIG. 4. a)-b) Pole figures of Cu {111} and Ta/TaN {101} of Cu5nm/Ta5nm x25 and Cu10nm/TaN3.5 NML x 8 in the as deposited state. c) and d) are the XRD pattern of the Cu/Ta and Cu/TaN NMLs respectively, collected in the as deposited and after different annealing treatments. The reference bulk reflections of Ta, Ta_2Si, Ta-β and TaN are also indicated as they are observed.

function of Cu thickness, period thickness (the bilayer thickness of two adjacent films), and the interface density, which is defined as the number of film interfaces per nanometer within the transverse direction of the multilayer region. As Cu is the most thermally conductive material within the NML system, a general increase in thermal conductivity is observed with increasing cumulative Cu layer thickness (5a). Correspondingly, the thermal conductivity increases in a similar manner as the total period thickness is increased (5b).

For a given period thickness, trends in the measured thermal conductivity are closely coupled to the Cu concentration of a given period, which can explain the behavior of films which appear to be outliers of the general trend. For example, for the Cu/Ta films, a large increase in the intrinsic thermal conductivity is observed in the 7 nm period case, which can be attributed to the fact that there is a 5/2 Cu/Ta ratio as opposed to a 1/1 ratio in the other Cu/Ta films. And similarly for the 13.5 nm period Cu/TaN sample, the increased thermal conductivity can be attributed to the 10/3.5 Cu/TaN ratio, which is a higher Cu concentration than in the other Cu/TaN period thicknesses. Individual films thicknesses for each NML system are tabulated and provided in the supplementary material (Table S3).

In contrast to the positive trends in 5(a) and 5(b), for the Cu/W NMLs, as the interface density is increased, there is an observable reduction in the overall thermal conductivity of the multilayer region due to the cumulative thermal resistance of the interfaces (5c). To quantify the conductance of the interfaces, the thermal boundary conductance is calculated in the same manner as in Refs. 53 and 54, in which the resistances of the individual layers and corresponding interfaces within the multilayer region are assumed to add in series. The average thermal boundary conductance of the multilayer system, G, is then considered as the mean resistance between adjacent layers within a period according to the equation:

$$G = 2\left[\frac{d_{Cu}+d_{film}}{\kappa_{measured}} - \frac{d_{Cu}}{\kappa_{Cu}} - \frac{d_{film}}{\kappa_{film}}\right]^{-1} \quad (1)$$

where $\kappa_{measured}$ is the measured thermal conductivity of the multilayer region, d_{Cu} and d_{film} are the thicknesses of adja-

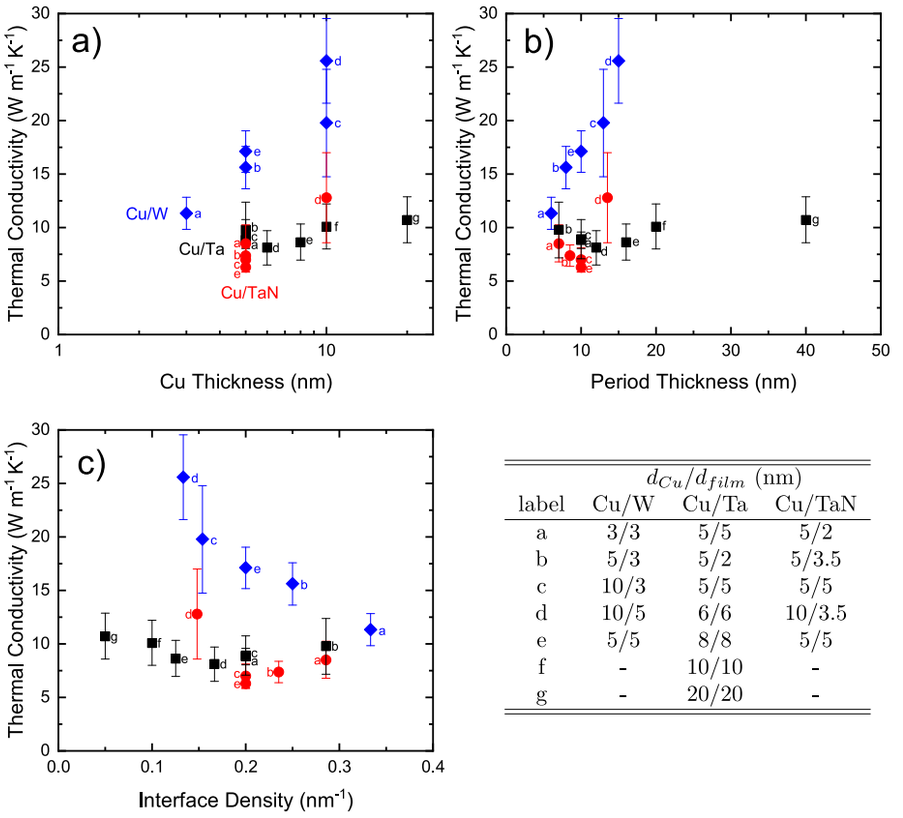

	d_{Cu}/d_{film} (nm)		
label	Cu/W	Cu/Ta	Cu/TaN
a	3/3	5/5	5/2
b	5/3	5/2	5/3.5
c	10/3	5/5	5/5
d	10/5	6/6	10/3.5
e	5/5	8/8	5/5
f	-	10/10	-
g	-	20/20	-

FIG. 5. Measured thermal conductivity of the NMLs as a function of a) Cu thickness (of a single period), b) period thickness, and c) interface density. The letters beside each data point are provided so that individual samples can be distinguished between each panel. For reference, the nominal period compositions are provided in the adjacent table. Complete details for each individual film are tabulated in Table S3 of the supplementary material.

cent layers, and κ_{Cu} and κ_{film} are corresponding bulk copper and adjacent film thermal conductivities. We note that the subscript, *film*, in this notation is in reference to the film adjacent to Cu (in this case, W). A series of films with different thicknesses of the respective pure metals were deposited on sapphire substrates to determine the bulk thermal conductivities of Cu and W. The thermal conductivities of the thickest films (600 nm) were measured with TDTR, and found to be 405 and 100 W m^{-1} K^{-1} for Cu and W, respectively (see supplementary material, Figure S4). Upon calculation of Equation 1, the average TBC for all Cu/W samples is found to be 3.9 $\pm$ 0.4 GW m^{-2} K^{-1} and does not demonstrate an observable dependence upon the interface density. For reference, this derived value is within the range of other copper-metal interfaces calculated through a similar approach; for example, Cheaito et al.[25] calculates the thermal boundary conductance between Cu/Nb multilayers as 4.7 GW m^{-2} K^{-1} while Gundrum et al.[26] find that of Cu/Al to be 3.7 GW m^{-2} K^{-1}.

While a clear reduction in thermal conductivity is observed with increasing interface density for the Cu/W NMLs, a negative trend in thermal conductivity is not observed for Cu/Ta and Cu/TaN NMLs, indicating that measurement of the multilayer systems is insensitive to the thermal boundary conductance, and thus calculation of the TBC via Equation 1 would not be applicable.

For further insight into expected differences in thermal boundary conductance between the different material interfaces, we consider values calculated from the electronic diffuse mismatch model (EDMM). This model assumes diffuse scattering of electrons at the interface and has been demonstrated as reasonably accurate at capturing trends in TBC, even at low temperatures[25,26,57,58]. Using the same analytical formalism outlined by Cheaito *et al.*[25], the thermal boundary conductance at a metal/metal interface can be expressed as:

$$G_{1/2} = 1/4\zeta_{1/2}C_{e,1}v_{F,1} \tag{2}$$

Where $\zeta_{1/2}$ is the transmission coefficient from layer 1 to layer 2, and $C_{e,1}$ and $v_{F,1}$ are the electronic heat capacity and Fermi velocity of layer 1. The product of $1/4C_{e,1}v_{F,1}$ is also defined as the derivative of the electronic energy flux at the interface $(\partial q_1/\partial T)$. The Electronic heat capacity of layer 1 is defined as $\pi^2/3D(E_{F,1})k_B^2T$, where k_B is the Boltzmann constant and $D(E_{F,1})$ is the density of states at the Fermi energy of layer 1. The transmission coefficient of the interface is then given as:

$$\zeta_{1/2} = \frac{D(E_{F,2})v_{F,2}}{D(E_{F,2})v_{F,2} + D(E_{F,1})v_{F,1}} \tag{3}$$

Using these equations, we calculate the expected thermal

boundary conductance for the elemental metals measured in this study (i.e. Cu, W, and Ta), for which the Fermi energy, velocity, and density of states are well defined. For reference, we tabulate the necessary parameters for the transmission coefficient calculation in Table II. In all cases, the density of states at the Fermi energy, as well as the Fermi velocity have been taken from literature. We note that in some cases, the Fermi velocity has been calculated from the Fermi energy, E_F, from the relation $v_F = \sqrt{2E_F/m}$, where m is the mass of an electron.

Metal	$D(E_F)$ (10^{47} m^{-3})	v_F (10^6 m s^{-1})
Cu	1.41[25]	1.12[25]
Ta	0.29[59]	1.83[59]
W	1.63[60]	1.43[61]
Interface$_{1/2}$	$\zeta_{1/2}$	G$_{1/2}$ (GW m^{-2} K^{-1})
Cu/Ta	0.25	1.85
Cu/W	0.60	4.36

TABLE II. Resultant transmission coefficients and thermal boundary conductance as calculated by the EDMM, outlined by Equations 2 and 3. For reference, the density of states and Fermi velocity values used in the calculations are also provided.

With these values, we calculate room-temperature thermal boundary counductances of 1.85 and 4.36 GW m^{-2} K^{-1} for Cu/Ta and Cu/W, respectively. Despite the simplicity of this analytical model, there is relatively good agreement with the experimentally determined TBC for Cu/W (for example, 3.9 $\pm$ 0.4 as opposed to 4.36 GW m^{-2} K^{-1} for the experimentally determined and theoretical values, respectively).

While TBC has been shown to be closely correlated with the derivative of the electronic energy flux at the interface[25], $\partial q_1/\partial T$, is the same as all metals are interfaced with copper. However, the transmission coefficient for Cu/W is found to be higher than that of Cu/Ta, which is attributed to the higher density of states at the Fermi energy in W, and thus gives rises to the higher overall TBC.

As an additional demonstration of the role of interfacial resistance on the thermal transport of the NMLs, we observe changes in the thermal conductivity as a function of annealing temperature, displayed in Figure 6. Cu/Ta, Cu/TaN, and Cu/W samples with a nominal period thickness of 10 nm, were each annealed at a constant temperature in the range of 500 - 800 °C. The total thickness of the multilayer regions were 238, 253.5, and 1000 nm for the Cu/Ta, Cu/TaN, and Cu/W multilayers, respectively. No change in thermal conductivity is observed for the anneals below 600 °C as the multilayer stack retains the integrity of its layered structure as described in previous section. However, while the NML structure does not degrade into a nanocomposite until annealing above 750 °C, recent works have demonstrated that subtle interface alterations occur at lower temperatures, which can subsequently impact carrier transport. For example, in a study by Powers *et al.*[16], it has been demonstrated that for anneals below 400 °C, interfaces within Cu/Ta NMLs retain a flat surface, while for temperatures above 600 °C, hillock formations have

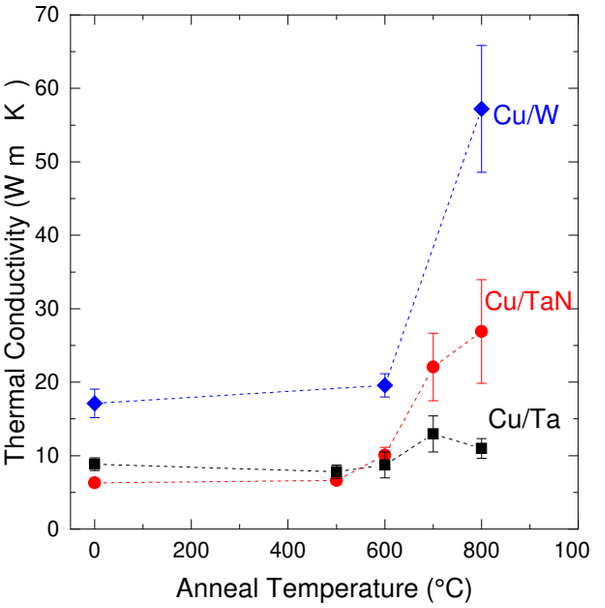

FIG. 6. Thermal conductivity of the Cu/Ta, Cu/TaN, and Cu/W multilayer regions as a function of anneal temperature. Prior to the anneal, the period thickness for each multilayer system was 10 nm, whereas the total multilayer thickness of the layer is 238, 253.5, and 1000 nm, for Cu/Ta, Cu/TaN, and Cu/W, respectively.

been observed. Furthermore, the NMLs within the figure are composed of 10 nm periods; in another recent work on Cu/W multilayer systems, Dong *et al.* have demonstrated that in systems with layers less than 12 nm, phonon transport also plays a non-negligible role. In the case of phonon transport, interfacial resistance is inherently linked to the overlap of phonon states between two adjacent materials; and therefore any intermixing of adjacent materials at the interface, could have an averaging effect on the vibrational spectra[63–66], thereby reducing the interfacial resistance, and increasing the measured thermal conductivity.

Outside of reductions in interfacial resistance, increases in the thermal conductivity at temperatures $\leq$ 700 °C could be correlated to the formation of lower resistivity phases. For example, XRD measurements of the annealed films demonstrate the formation of α-Ta by 600 °C in the Cu/Ta multilayers (Figure 4c), and TaN$_{0.5}$ in the Cu/Ta at 700 °C (Figure 4d). The film resistivity can, in some cases, be reduced by an order of magnitude or more, such as in the case of β-Ta to α-Ta as discussed by Wang *et al.*[67] and Grosser *et al.*[68] and investigated through first-principles calculations by Lanzillo *et al.*[10]. As the electronic contribution to thermal conductivity is inversely proportional to the thermal conductivity through the Wiedemann-Franz law, a corresponding increase in thermal conductivity would be expected with the onset of these lower resitivity phases.

Once the annealing temperature approaches 800 °C, the layered structure of the multilayer region is lost as there is significant diffusion between the Cu and W, Ta, or TaN films. As such, there is a reduction in the interface density of the region,

and the thermal conductivity is enhanced. While all samples display an increase in thermal conductivity as a function of the annealing temperature, a slight decrease is observed for the Cu/Ta NML annealed at 800 °C. As previously discussed in the XRD results, at 800 °C, the formation of Ta silicate phases are observed, indicating Si diffusion from the substrate into NML region. The presence of Ta silicate in the region could prove as a source of alloy scattering, and could consequently be responsible for the reduction in measured thermal conductivity.

IV. CONCLUSION

In summary, a comprehensive comparison has been prepared for Cu-based nanomultilayers. NMLs were grown over a range of layer and period thicknesses for films of Cu/Ta, Cu/TaN, and Cu/W, and the thermal and structural properties of the films were characterized through TDTR, SEM, and XRD measurements. For further insight into the role of the NML structure upon thermal transport, samples were annealed to the point of layer diffusion, yielding significant increases in the measured thermal conductivity, demonstrating the critical role of interfacial resistance on thermal transport within these systems.

AUTHOR CONTRIBUTIONS

Claudia Cancellieri and Ethan A. Scott contributed equally to this work.

SUPPLEMENTARY MATERIAL

See supplementary material for additional details on XRD, AFM, sheet resistance measurements, sensitivity analyses of the measured thermal properties, as well as tabulated values of the thermophysical properties of the samples in this study.

ACKNOWLEDGEMENTS

The authors are thankful to Dr. H. Ruedi for his help on performing thermal treatments. This manuscript is based upon work supported by the Air Force Office of Scientific Research under Award No. FA9550-18-1-0352.

DATA AVAILABILITY

The data that supports the findings of this study are available from the corresponding author upon reasonable request.

[1]D. Gall, J. Appl. Phys. **127**, 050901 (2020).
[2]R. S. Smith, E. T. Ryan, C.-K. Hu, K. Motoyama, N. Lanzillo, D. Metzler, L. Jiang, J. Demarest, R. Quon, L. Gignac, C. Breslin, A. Giannetta, and S. Wright, AIP Adv. **9**, 025015 (2019).
[3]D. Valencia, E. Wilson, Z. Jiang, G. A. Valencia-Zapata, K.-C. Wang, G. Klimeck, and M. Povolotskyi, Phys. Rev. Appl. **9**, 044005 (2018).
[4]N. A. Lanzillo, O. D. Restrepo, P. S. Bhosale, E. Cruz-Silva, C.-C. Yang, B. Youp Kim, T. Spooner, T. Standaert, C. Child, G. Bonilla, and K. V. R. M. Murali, Appl. Phys. Lett. **112**, 163107 (2018).
[5]N. A. Lanzillo, J. Appl. Phys. **121**, 175104 (2017).
[6]S. M. Merchant, S. H. Kang, M. Sanganeria, B. van Schravendijk, and T. Mountsier, JOM **53**, 43 (2001).
[7]J. Kriz, C. Angelkort, M. Czekalla, S. Huth, D. Meinhold, A. Pohl, S. Schulte, A. Thamm, and S. Wallace, Microelectron. Eng. **85**, 2128 (2008).
[8]M. W. Lane, C. E. Murray, F. R. McFeely, P. M. Vereecken, and R. Rosenberg, Appl. Phys. Lett. **83**, 2330 (2003).
[9]M. Wislicenus, R. Liske, L. Gerlich, B. Vasilev, and A. Preusse, Microelectron. Eng. **137**, 11 (2015).
[10]N. A. Lanzillo, L. Clevenger, R. R. Robison, and D. C. Edelstein, J. Appl. Phys. **127**, 125705 (2020).
[11]L. P. Jeurgens, Z. Wang, and E. J. Mittemeijer, International Journal of Materials Research **100**, 1281 (2009).
[12]F. Spaepen, Acta Materialia **48**, 31 (2000).
[13]T. W. Barbee, in *Symposium V – Application of Synchrotron Radiation Techniques. . . IV*, MRS Proceedings, Vol. 524 (1998) p. 145 (7 pages).
[14]J. Xue, Y. Li, L. Gao, D. Qian, Z. Song, X. Wang, X. Zhu, and J. Chen, Surf. Coat. Technol. **381**, 125179 (2020).
[15]L. Dong, G. Wei, T. Cheng, J. Tang, X. Ye, M. Hong, L. Hu, R. Yin, S. Zhao, G. Cai, Y. Shi, B. Pan, C. Jiang, and F. Ren, ACS Appl. Mater. Interfaces **12**, 8886 (2020).
[16]M. Powers, B. Derby, E. Raeker, N. Champion, and A. Misra, Thin Solid Films **693**, 137692 (2020).
[17]A. Giri and P. E. Hopkins, Adv. Funct. Mater. **30**, 1903857 (2020).
[18]T. Zhan, K. Oda, S. Ma, M. Tomita, Z. Jin, H. Takezawa, K. Mesaki, Y.-J. Wu, Y. Xu, T. Matsukawa, T. Matsuki, and T. Watanabe, ACS Appl. Mater. Interfaces **12**, 22347 (2020).
[19]A. Every, Y. Tzou, D. Hasselman, and R. Raj, Acta Metallurgica et Materialia **40**, 123 (1992).
[20]C.-W. Nan, R. Birringer, D. R. Clarke, and H. Gleiter, J. Appl. Phys. **81**, 6692 (1997).
[21]F. Moszner, C. Cancellieri, M. Chiodi, S. Yoon, D. Ariosa, J. Janczak-Rusch, and L. P. H. Jeurgens, Acta Mater. **107**, 345 (2016).
[22]C. Cancellieri, F. Moszner, M. Chiodi, S. Yoon, J. Janczak-Rusch, and L. P. H. Jeurgens, Journal of Applied Physics **120**, 195107 (2016), https://doi.org/10.1063/1.4967992.
[23]A. V. Druzhinin, D. Ariosa, S. Siol, N. Ott, B. B. Straumal, J. Janczak-Rusch, L. P. H. Jeurgens, and C. Cancellieri, Materialia **7**, 100400 (2019).
[24]H.-J. Lee, K.-W. Kwon, C. Ryu, and R. Sinclair, Acta Mater. **47**, 3965 (1999).
[25]R. Cheaito, K. Hattar, J. T. Gaskins, A. K. Yadav, J. C. Duda, T. E. Beechem, J. F. Ihlefeld, E. S. Piekos, J. K. Baldwin, A. Misra, and P. E. Hopkins, Applied Physics Letters **106** (2015), 10.1063/1.4913420.
[26]B. C. Gundrum, D. G. Cahill, and R. S. Averback, Physical Review B - Condensed Matter and Materials Physics **72**, 245426 (2005).
[27]P. E. Hopkins, T. E. Beechem, J. C. Duda, J. L. Smoyer, and P. M. Norris, Appl. Phys. Lett. **96**, 011907 (2010).
[28]B. M. Clemens, G. L. Eesley, and C. A. Paddock, Phys. Rev. B **37**, 1085 (1988).
[29]S. W. King, M. French, M. Jaehnig, M. Kuhn, B. Boyanov, and B. French, Journal of Vacuum Science & Technology B, Nanotechnology and Microelectronics: Materials, Processing, Measurement, and Phenomena **29**, 051207 (2011).
[30]A. Schmidt, *Optical Characterization of Thermal Transport from the Nanoscale to the Macroscale*, Dissertation, Massachusetts Institute of Technology (2008).
[31]D. G. Cahill, Review of Scientific Instruments **75**, 5119 (2004).
[32]D. G. Cahill, K. E. Goodson, and A. Majumdar, Journal of Heat Transfer **124**, 223 (2002).
[33]P. E. Hopkins, J. R. Serrano, L. M. Phinney, S. P. Kearney, T. W. Grasser, and C. T. Harris, Journal of Heat Transfer **132**, 081302 (2010).
[34]Y. Touloukian and E. Buyco, *Thermophysical Properties of Matter—Specific Heat: Nonmetallic Solids, Vol. 5*, edited by Y. Touloukian and C. Ho (IFI/Plenum, New York, 1970).

[35]A. Sood, R. Cheaito, T. Bai, H. Kwon, Y. Wang, C. Li, L. Yates, T. Bougher, S. Graham, M. Asheghi, M. Goorsky, and K. E. Goodson, Nano Letters **18**, 3466 (2018).
[36]E. A. Scott, S. W. Smith, M. D. Henry, C. M. Rost, A. Giri, J. T. Gaskins, S. S. Fields, S. T. Jaszewski, J. F. Ihlefeld, and P. E. Hopkins, Applied Physics Letters **113** (2018), 10.1063/1.5052244.
[37]P. E. Hopkins, L. M. Phinney, J. R. Serrano, and T. E. Beechem, Physical Review B - Condensed Matter and Materials Physics **82**, 085307 (2010).
[38]W. F. Giauque and P. F. Meads, Journal of the American Chemical Society **63**, 1897 (1941).
[39]P. Nath and K. Chopra, Thin Solid Films **20**, 53 (1974).
[40]A. Tesfamicha and A. D. Woldeyo, Asian Journal of Scientific Research **6**, 339 (2013).
[41]J. Bryner, D. M. Profunser, J. Vollmann, E. Mueller, and J. Dual, Ultrasonics **44**, e1269 (2006).
[42]E. Bozorg-Grayeli, Z. Li, M. Asheghi, G. Delgado, A. Pokrovsky, M. Panzer, D. Wack, and K. E. Goodson, Applied Physics Letters **99**, 261906 (2011).
[43]C. H. Mastrangelo, T. Yu-Chong, and R. S. Muller, Sensors and Actuators A: Physical **23**, 856 (1990).
[44]J. T. Gaskins, P. E. Hopkins, D. R. Merrill, S. R. Bauers, E. Hadland, D. C. Johnson, D. Koh, J. H. Yum, S. Banerjee, B. J. Nordell, M. M. Paquette, A. N. Caruso, W. A. Lanford, P. Henry, L. Ross, H. Li, L. Li, M. French, A. M. Rudolph, and S. W. King, ECS Journal of Solid State Science and Technology **6**, N189 (2017).
[45]N. Stojanovic, J. Yun, J. M. Berg, M. Holtz, and H. Temkin, **16**, 639 (2009).
[46]J. L. Braun, D. H. Olson, J. T. Gaskins, and P. E. Hopkins, Review of Scientific Instruments **90** (2019), 10.1063/1.5056182.
[47]G. White and S. Collocott, Journal of Physical and Chemical Reference Data **13**, 1251 (1984).
[48]J. Hostetler, A. Smith, and P. Norris, Microscale Thermophysical Engineering **1**, 237 (1997).
[49]C. Thompson, Acta Metallurgica **36**, 2929 (1988).
[50]B. M. Clemens and J. G. Gay, Phys. Rev. B **35**, 9337 (1987).
[51]K. Holloway, P. M. Fryer, C. Cabral, J. M. E. Harper, P. J. Bailey, and K. H. Kelleher, Journal of Applied Physics **71**, 5433 (1992), https://doi.org/10.1063/1.350566.
[52]R. Hübner, M. Hecker, N. Mattern, V. Hoffmann, K. Wetzig, C. Wenger, H.-J. Engelmann, C. Wenzel, E. Zschech, and J. Bartha, Thin Solid Films **437**, 248 (2003).
[53]Y. K. Koh, Y. Cao, D. G. Cahill, and D. Jena, Adv. Funct. Mater. **19**, 610 (2009).
[54]A. Giri, S. W. King, W. A. Lanford, A. B. Mei, D. Merrill, L. Li, R. Oviedo, J. Richards, D. H. Olson, J. L. Braun, J. T. Gaskins, F. Deangelis, A. Henry, and P. E. Hopkins, Advanced Materials **30**, 1804097 (2018).
[55]D. A. Samoshkin, I. V. Savchenko, S. V. Stankus, and A. S. Agazhanov, Thermophysics and Aeromechanics **25**, 735 (2018).
[56]W. S. Williams, JOM **50**, 62 (1998).
[57]R. B. Wilson and D. G. Cahill, Phys. Rev. Lett. **108**, 255901 (2012).
[58]C. B. Saltonstall, Z. D. McClure, M. J. Abere, D. Guzman, S. T. Reeve, A. Strachan, P. G. Kotula, D. P. Adams, and T. E. Beechem, Phys. Rev. B **101**, 245422 (2020).
[59]L. F. Mattheiss, Phys. Rev. B **1**, 373 (1970).
[60]Z. Lin, L. V. Zhigilei, and V. Celli, Phys. Rev. B **77**, 075133 (2008).
[61]M. S. Sodha and P. K. Dubey, J. Phys. D: Appl. Phys. **3**, 139 (1970).
[62]D. Li, F. Tian, D. Duan, K. Bao, B. Chu, X. Sha, B. Liu, and T. Cui, RSC Adv. **4**, 10133 (2014).
[63]R. J. Stevens, L. V. Zhigilei, and P. M. Norris, Int. J. Heat Mass Transfer **50**, 3977 (2007).
[64]Z. Liang and H.-L. Tsai, J. Phys.: Condens. Matter **23**, 495303 (2011).
[65]T. S. English, J. C. Duda, J. L. Smoyer, D. A. Jordan, P. M. Norris, and L. V. Zhigilei, Phys. Rev. B **85**, 035438 (2012).
[66]Z. Tian, K. Esfarjani, and G. Chen, Phys. Rev. B **86**, 235304 (2012).
[67]W.-L. Wang, W.-C. Chen, K.-T. Peng, H.-C. Kuo, M.-H. Yeh, H.-J. Chien, and T.-H. Ying, Thin Solid Films **603**, 34 (2016).
[68]M. Grosser and U. Schmid, Thin Solid Films **517**, 4493 (2009).

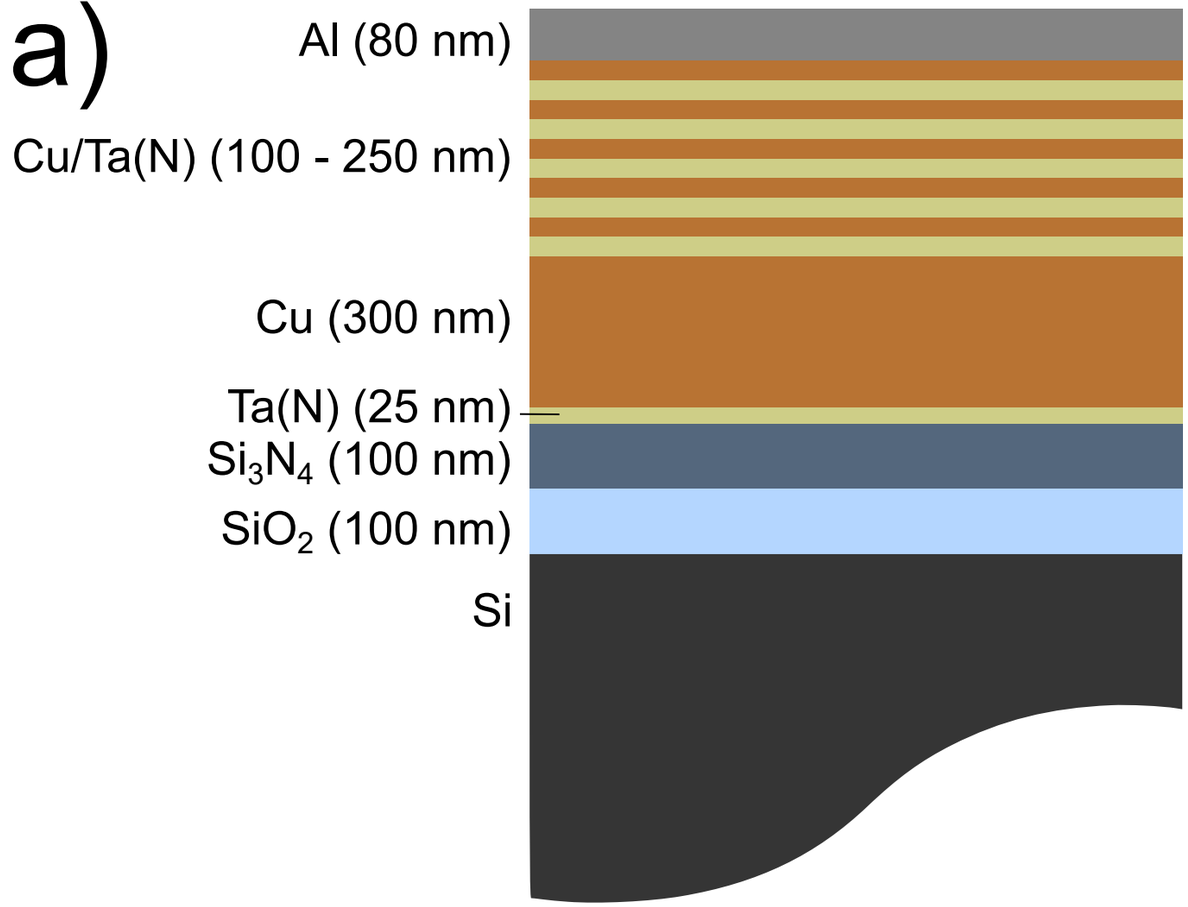

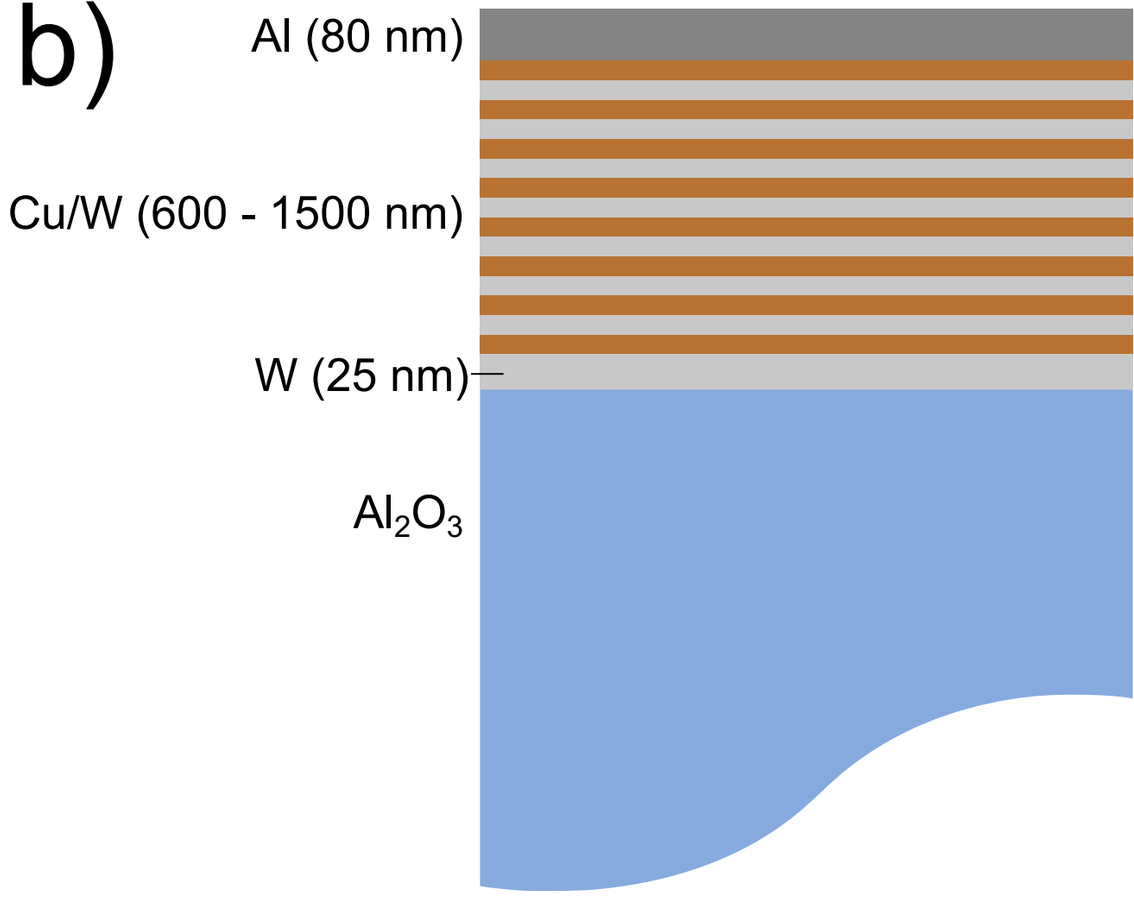

Journal of Applied Physics

AIP Publishing

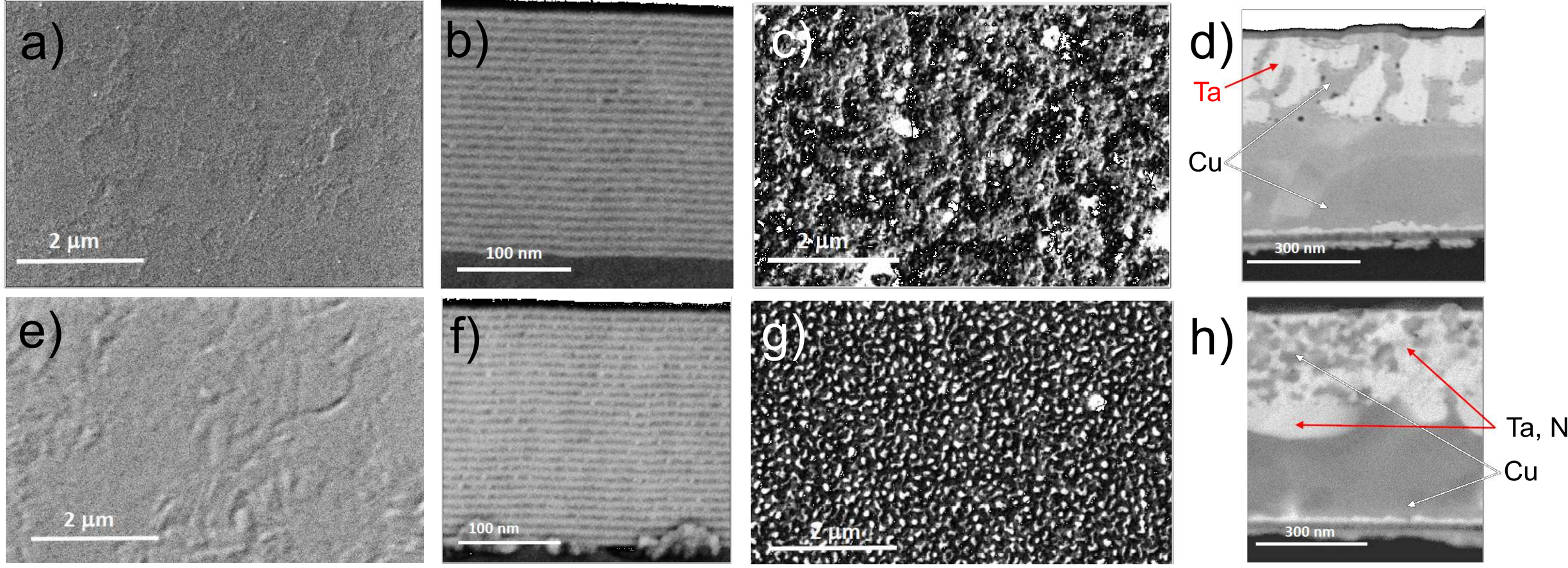

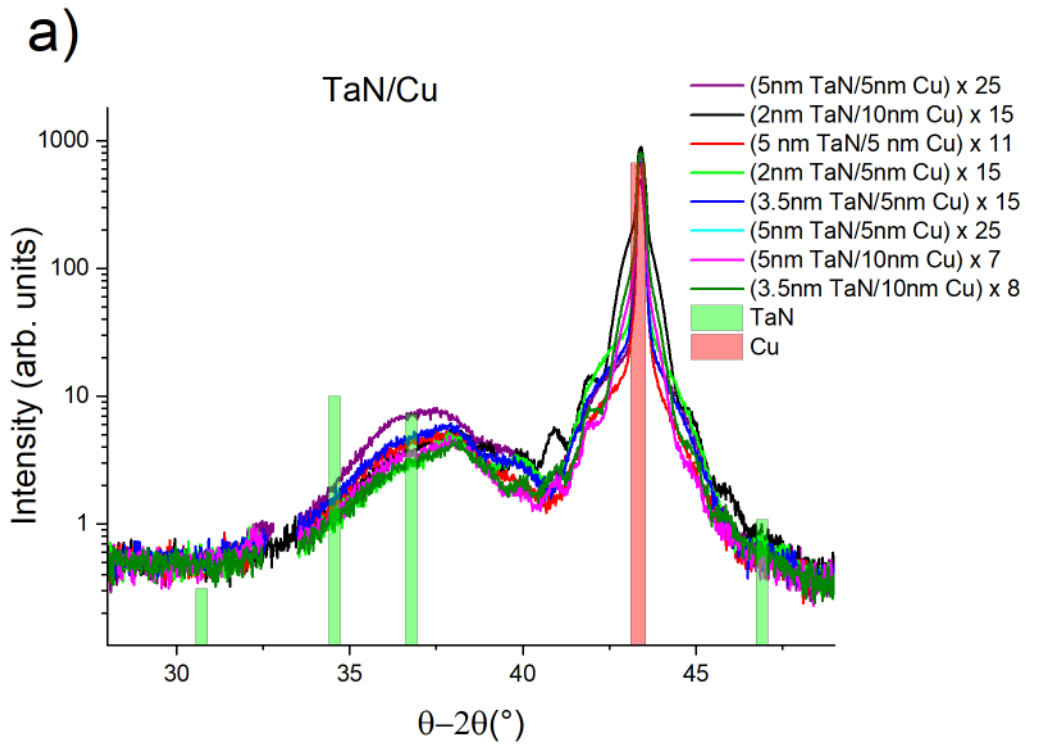

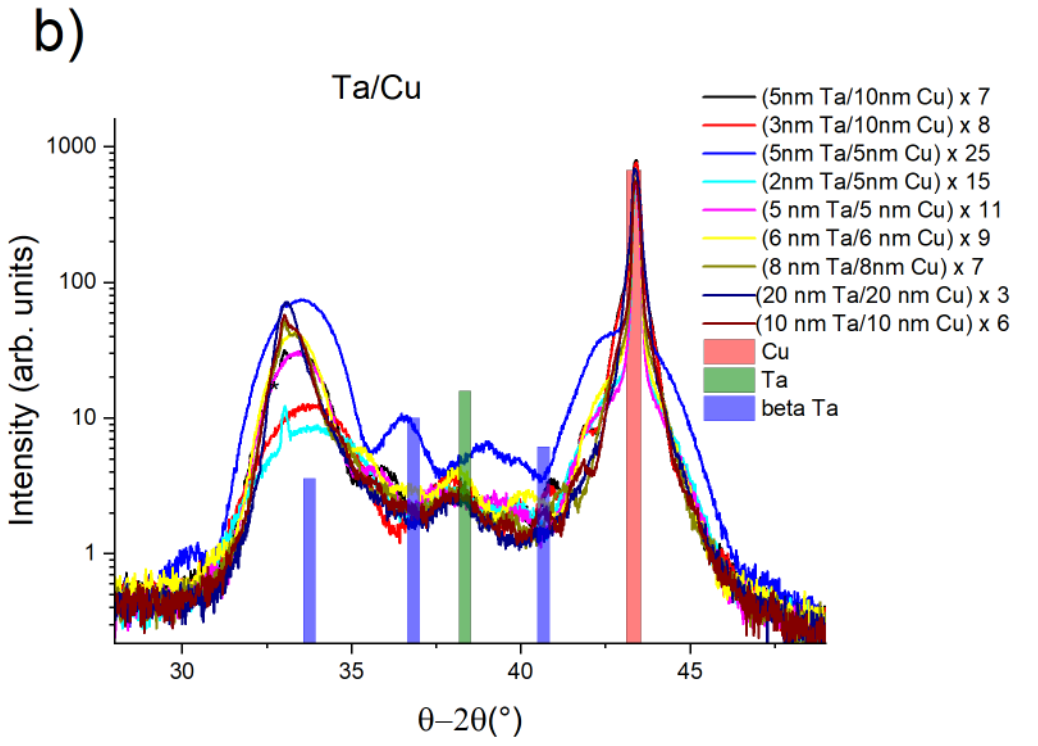

a)

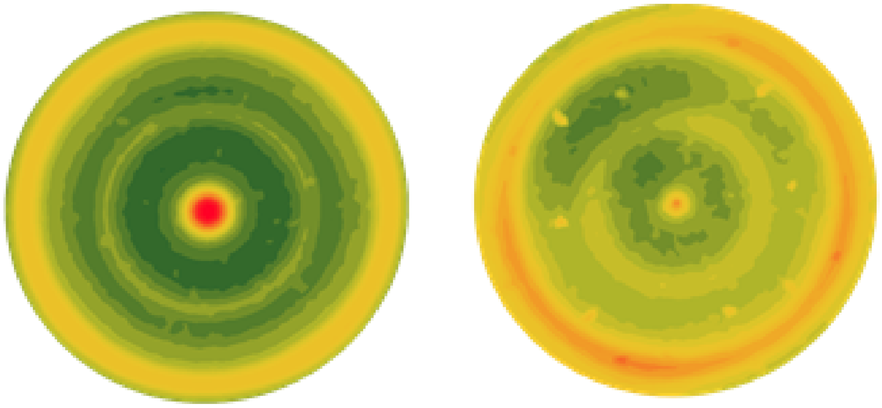

b)

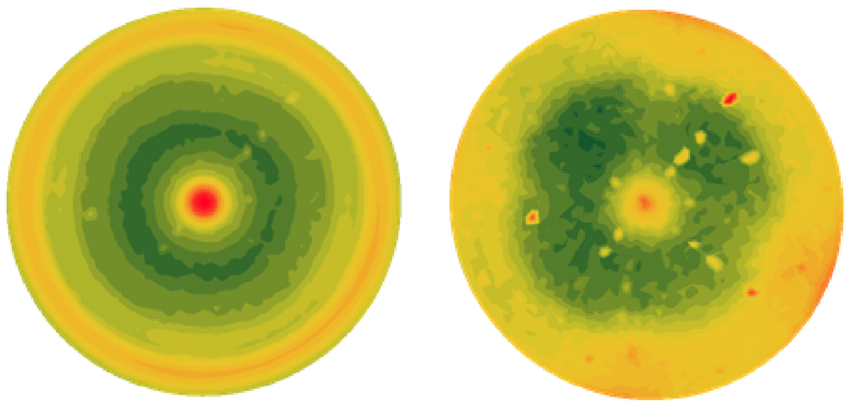

c)

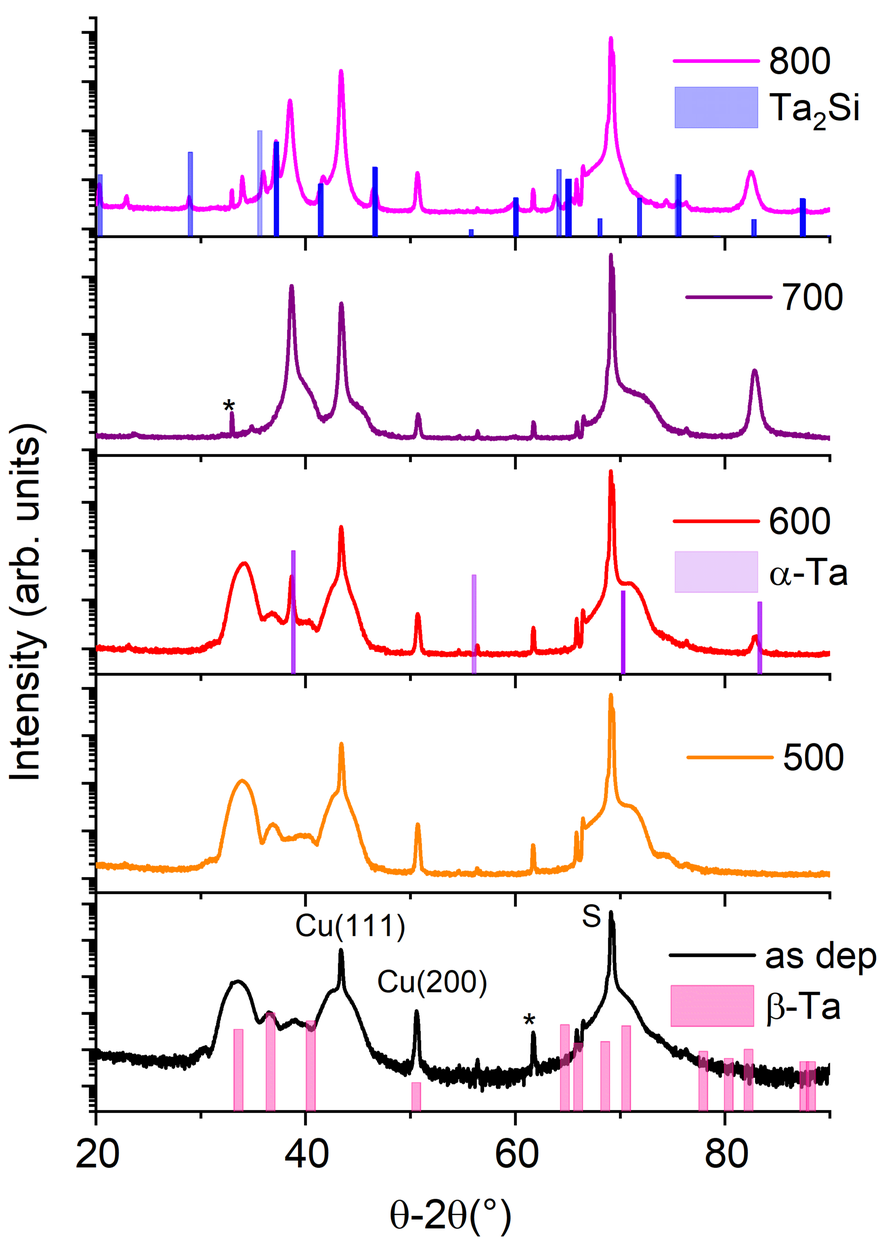

d)

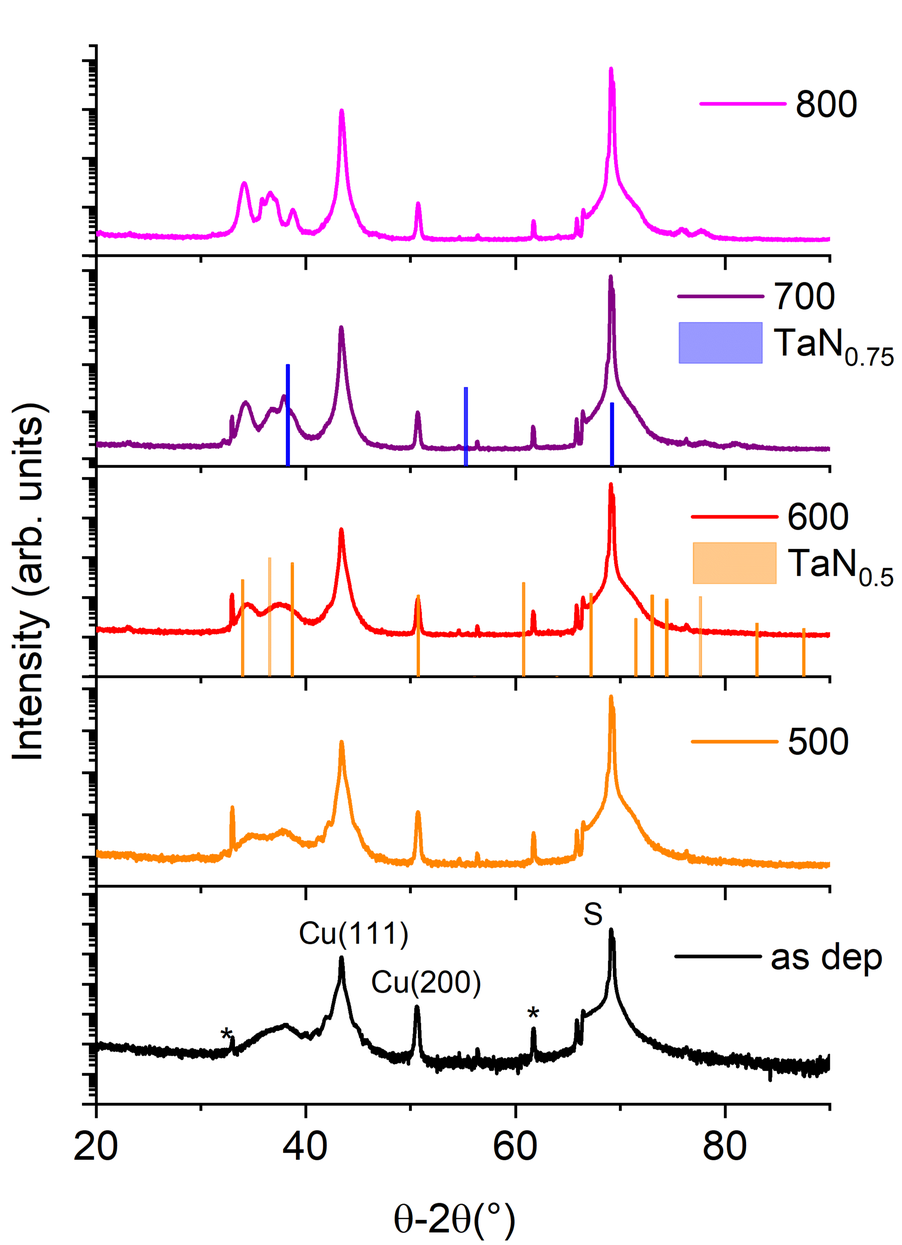

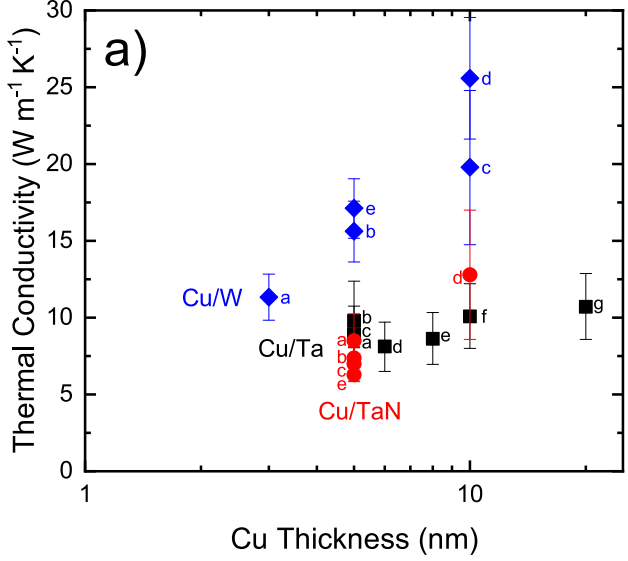

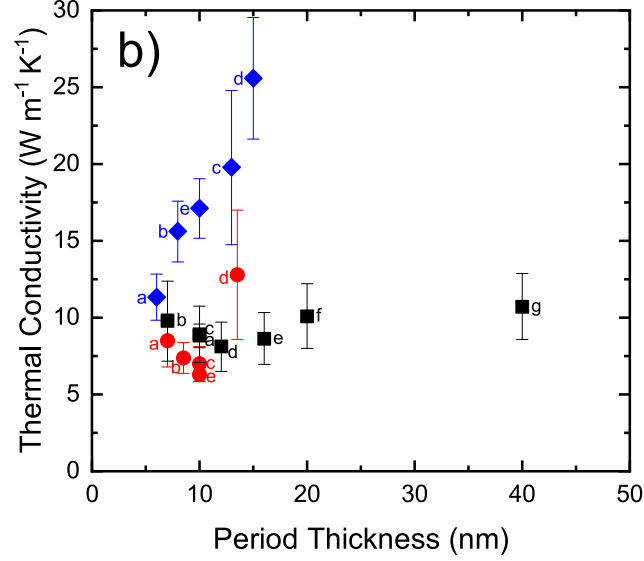

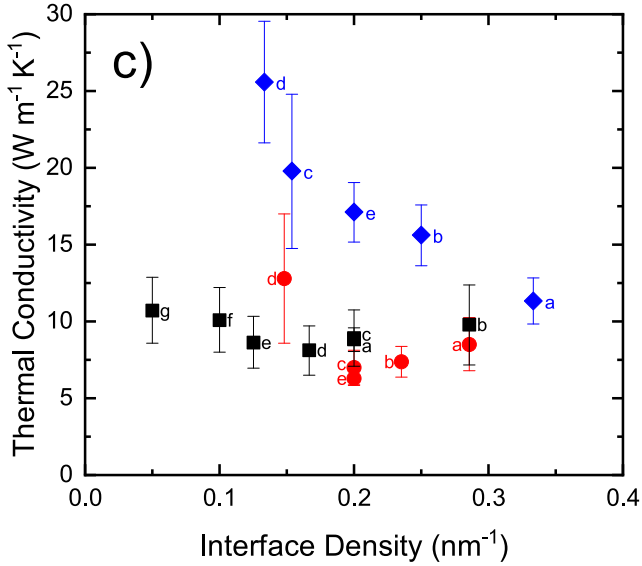

	d_{Cu}/d_{film} (nm)		
label	Cu/W	Cu/Ta	Cu/TaN
a	3/3	5/5	5/2
b	5/3	5/2	5/3.5
c	10/3	5/5	5/5
d	10/5	6/6	10/3.5
e	5/5	8/8	5/5
f	-	10/10	-
g	-	20/20	-